

TWO-SCALE POLARIMETRIC EMISSIVITY MODEL: EFFICIENCY IMPROVEMENTS AND COMPARISONS WITH DATA

D. R. Lyzenga

Department of Naval Architecture and Marine Engineering
University of Michigan
Ann Arbor, MI, USA

J. F. Vesecky

Department of Electrical Engineering
University of California
Santa Cruz, CA, USA
and
Atmospheric, Oceanic and Space Science Department
University of Michigan
Ann Arbor, MI, USA

Abstract—The two-scale model provides a framework for explaining the polarization and angular dependence of the microwave radiation emitted from the ocean surface. In this model the surface is viewed as a collection of randomly oriented facets. The emissivity of each facet is calculated using the small perturbation method (SPM), and that of the entire surface is obtained by integrating the local emissivity over all possible surface slopes, weighted by the probability of encountering these slopes. Since each SPM calculation involves a double integral, the model requires in principle the evaluation of a four-dimensional integral. This paper explores two methods for reducing the computational time required by the two-scale model. In one version, the azimuthal dependence of the local emissivity is represented by a truncated Fourier series and slope integral is computed numerically. In the second version the slope integral is carried out analytically, after expanding the integrand as a Taylor series in the surface slope. Hydrodynamic modulation effects are included in order to explain the upwind-downwind asymmetry of the emissivity. The calculated emissivities from the two versions of the model are compared with each other and with airborne and spaceborne measurements.

- 1 Introduction**
- 2 The Two-Scale Model**
- 3 Analytical Evaluation of Slope Integral**
- 4 Hydrodynamic Modulation Effects**
- 5 Comparison of Numerical and Analytical Results**
- 6 Comparisons with Experimental Data**
- 7 Conclusions**

Acknowledgment

Appendix A. Analytical Expressions for Fourier Harmonics

References

1. INTRODUCTION

The microwave emissivity of the ocean surface is influenced by both the small-scale and the large-scale surface roughness. Many features of the emissivity are accounted for by the geometric optics (GO) model, which takes account of surface elements with length scales much longer than the wavelength of the microwave radiation [1–4]. However, several aspects of the emissivity also appear to require the small-scale roughness to be accounted for. The two-scale model described by Yueh [5] accounts for both length scales, but is computationally intensive. The larger scales are accounted for by integrating the local emissivity over all surface slopes, as in the geometric optics model. In addition, small-scale surface roughness effects, which are ignored by the GO model, are included by using the small perturbation method (SPM) to compute the local emissivity. Unfortunately, since the SPM involves a double integral for each local surface slope, a four-dimensional integration is required for each Stokes parameter. The large number of calculations required for a single evaluation of this model limits its usefulness for wind speed inversion algorithms which involve repeated model evaluations.

The efficiency of the model can be improved by using analytical expressions for the angular dependence of the local emissivity. The dependence of the emissivity on the local azimuthal angle is known to be very well approximated by a second-order Fourier expansion. The use of such an expansion allows a considerable reduction in computing time with virtually no loss in accuracy. The dependence on the local

incidence angle is more problematic, but we have explored the use of a Taylor expansion to speed up the computation even further. These approximations are described in the following sections, and the results are compared with available measurements.

2. THE TWO-SCALE MODEL

In the two-scale model, the brightness temperature for each polarization is given by

$$\bar{T}_b = \int_{-\infty}^{\infty} \int_{-\infty}^{\infty} T_b(\eta_x, \eta_y) p(\eta_x, \eta_y) a(\eta_x) d\eta_x d\eta_y \quad (1)$$

where $T_b(\eta_x, \eta_y)$ is the brightness temperature for a surface element with slopes η_x and η_y , $p(\eta_x, \eta_y)$ is the slope probability density function, and the factor

$$a(\eta_x) = \begin{cases} 1 - \eta_x \tan \theta & \eta_x < \cot \theta \\ 0 & \eta_x > \cot \theta \end{cases} \quad (2)$$

accounts for the projected area of a facet in the line of sight direction (the viewing direction is assumed to be in the positive x - z plane, at an angle θ with respect to the z axis). The local brightness temperature is a function of the surface slope because of two effects: (1) the change in the local incidence and azimuth angles, and (2) the rotation of the polarization basis vectors in the local coordinate system relative to those in the global coordinate system.

The local incidence angle is given by $\cos \theta' = \hat{n} \cdot \hat{k}$ where \hat{n} is the local surface normal and \hat{k} is the unit vector in the direction of observation. The local azimuth angle (relative to the wind direction) is given by

$$\tan \phi' = \frac{n_z \sin \phi \sin \theta + (n_x \sin \phi - n_y \cos \phi) \cos \theta}{\cos \phi \sin \theta - (n_x \cos \phi - n_y \sin \phi) \cos \theta'} \quad (3)$$

where n_z is the vertical component of the surface normal, n_x and n_y are the components in the plane of incidence and in the direction normal to the plane of incidence, respectively, and ϕ is the global azimuth angle or look direction relative to the wind direction.

The angle of rotation (α) between the polarization basis vectors in the local and global coordinate systems is given by $\sin \alpha = n_y / \sin \theta'$. Because of this rotation, electromagnetic radiation that is polarized along one of the principal axes in the global coordinate system contains

a mixture of polarizations in the local coordinate system, and vice versa. Thus, the brightness temperature as measured in the global coordinate system for a facet with slopes η_x and η_y can be written as

$$\begin{aligned} T_v(\eta_x, \eta_y) &= T'_v \cos^2 \alpha + T'_h \sin^2 \alpha - U' \sin \alpha \cos \alpha. \\ T_h(\eta_x, \eta_y) &= T'_h \cos^2 \alpha + T'_v \sin^2 \alpha + U' \sin \alpha \cos \alpha \\ \text{and } U(\eta_x, \eta_y) &= U' \cos 2\alpha + (T'_h - T'_v) \sin 2\alpha. \end{aligned} \quad (4)$$

where T'_v , T'_h , and U' are the local Stokes parameters (the fourth Stokes parameter, V , is invariant to rotations, and is therefore the same in the global and local coordinate systems). The local Stokes parameters may be considered as consisting of a geometric-optics component plus a correction for small-scale surface roughness effects. The geometric-optics temperatures can be written as and where and are the Fresnel reflection coefficients and is the physical surface temperature. The contributions due to small-scale surface roughness effects can be written as

$$T_{v0}(\theta') = T_s \left[1 - |R_v(\theta')|^2 \right] \quad \text{and} \quad T_{h0}(\theta') = T_s \left[1 - |R_h(\theta')|^2 \right]$$

where R_v and R_h are the Fresnel reflection coefficients and T_s is the physical surface temperature. The contributions due to small-scale surface roughness effects can be written as

$$\begin{bmatrix} T_{v1} \\ T_{h1} \\ U_1 \\ V_1 \end{bmatrix} = T_s \begin{bmatrix} R_v^{(1)} + 2\text{Re} \left\{ R_v R_{vv}^{(2)*} \right\} \\ R_h^{(1)} + 2\text{Re} \left\{ R_h R_{hh}^{(2)*} \right\} \\ 2\text{Re} \left\{ R_c^{(1)} + R_{vh}^{(2)} R_h^* + R_v R_{hv}^{(2)*} \right\} \\ 2\text{Im} \left\{ R_c^{(1)} + R_{vh}^{(2)} R_h^* + R_v R_{hv}^{(2)*} \right\} \end{bmatrix} \quad (5)$$

where

$$\begin{aligned} R_p^{(1)} &= \iint_{\Omega} g_p^{(1)}(k_x + k_r, k_y) W(k_x, k_y) dk_x dk_y, \\ R_{pq}^{(2)} &= \int_{-\infty}^{\infty} \int_{-\infty}^{\infty} g_{pq}^{(2)}(k_x + k_r, k_y) W(k_x, k_y) dk_x dk_y, \end{aligned}$$

$W(k_x, k_y)$ is the wave height spectrum, and Ω is the region defined by $(k_x + k \sin \theta)^2 + k_y^2 \leq k^2$ where k is the electromagnetic wavenumber

(Yueh [5, 6]). The dependence of these terms on the look direction or azimuthal angle is accurately represented by the truncated Fourier series

$$\begin{aligned} T_v(\theta, \phi) &= a_{v0} + a_{v1} \cos \phi + a_{v2} \cos 2\phi, \\ T_h(\theta, \phi) &= a_{h0} + a_{h1} \cos \phi + a_{h2} \cos 2\phi, \\ U(\theta, \phi) &= b_{U1} \sin \phi + b_{U2} \sin 2\phi, \quad \text{and} \\ V(\theta, \phi) &= b_{V1} \sin \phi + b_{V2} \sin 2\phi \end{aligned} \quad (6)$$

where ϕ is the angle between the look direction and the wind direction. Since this dependence is due entirely to the azimuthal dependence of the wave spectrum, the Fourier coefficients can be obtained by replacing the wave spectrum in the above expressions by

$$\begin{aligned} W_{a0}(k_x, k_y) &= \frac{1}{2\pi} \int_0^{2\pi} W(k_x, k_y) d\phi \quad \text{for } a_{v0} \text{ and } a_{h0}, \\ W_{a2}(k_x, k_y) &= \frac{1}{\pi} \int_0^{2\pi} W(k_x, k_y) \cos(2\phi) d\phi \quad \text{for } a_{v2} \text{ and } a_{h2}, \\ \text{and } W_{b2}(k_x, k_y) &= \frac{1}{\pi} \int_0^{2\pi} W(k_x, k_y) \sin(2\phi) d\phi \quad \text{for } b_{v2} \text{ and } a_{h2}. \end{aligned} \quad (7)$$

Because of the symmetry of the wave spectrum, the first harmonics (a_{v1} , a_{h1} , b_{U1} , and b_{V1}) are identically zero. Thus, only a few double integrals are required for each local incidence angle. The slope integral (1) is evaluated numerically by computing and storing the harmonic coefficients (a_{v0} , a_{h0} , a_{v2} , a_{h2} , b_{v2} , and b_{h2}) for each local incidence angle. For a given slope, the local incidence and azimuth angles are computed, the harmonic coefficients are obtained by interpolating the tabulated values, and the local emissivity is computed by evaluating the Fourier series (7).

3. ANALYTICAL EVALUATION OF SLOPE INTEGRAL

The slope integral (1), can be evaluated analytically by first expanding each of the local Stokes parameters as a Taylor series in the surface slope, i.e.,

$$T_b(\eta_x, \eta_y) = T_{b00} + T_{b10}\eta_x + T_{b01}\eta_y + T_{b11}\eta_x\eta_y + T_{b20}\eta_x^2 + T_{b02}\eta_y^2 + \dots \quad (8)$$

where the coefficients are obtained by taking the derivatives of T_b with respect to η_x and η_y . The derivatives of the geometric-optics components can be readily found (up to second order), but the derivatives of the SPM components are much more difficult to obtain. Because the SPM contributions are much smaller in magnitude than the geometric optics contributions, a fairly good approximation is to neglect the derivatives of the SPM terms in this expansion. However, these derivatives turn out to be important in conjunction with the hydrodynamic modulation effects discussed in the following section. We have therefore resorted to computing the first derivatives of the SPM components numerically. Analytical expressions for the Fourier harmonic coefficients obtained from this approximation are given in Appendix A, and comparisons with numerical results are presented in Section 5.

4. HYDRODYNAMIC MODULATION EFFECTS

The contributions to the brightness temperatures due to small-scale surface roughness effects are proportional to the short wave spectral density $W(k_x, k_y)$. Spatial variations in this spectral density can be described by means of the modulation transfer function (mtf) $m = m_r + im_i$, which is defined such that the fractional change in the short wave spectrum is given by

$$f(x, y) = \text{Re} \iint m k \psi(k_x, k_y) e^{i(k_x x + k_y y)} dk_x dk_y \quad (9)$$

where $\psi(k_x, k_y)$ is the one-sided Fourier transform of the surface elevation. The surface slopes in the upwind and crosswind directions can similarly be written as

$$\eta_u(x, y) = \text{Re} \iint i k_u \psi(k_x, k_y) e^{i(k_x x + k_y y)} dk_x dk_y$$

and (10)

$$\eta_c(x, y) = \text{Re} \iint i k_c \psi(k_x, k_y) e^{i(k_x x + k_y y)} dk_x dk_y$$

where $k_u = k_x \cos \phi + k_y \sin \phi$ and $k_c = k_y \cos \phi - k_x \sin \phi$. Using the properties

$$\langle \psi(k_x, k_y) \psi(k'_x, k'_y) \rangle = 0$$

and

$$\langle \psi(k_x, k_y) \psi^*(k'_x, k'_y) \rangle = S(k_x, k_y) \delta(k_x - k'_x) \delta(k_y - k'_y)$$

where $S(k_x, k_y)$ is the one-sided (large-scale) wave height spectrum, the correlations between the short wave spectrum and the surface slopes are then given by

$$\begin{aligned}\langle f\eta_u \rangle &= \frac{1}{2} \iint m_i k k_u S(k_x, k_y) dk_x dk_y \\ \langle f\eta_c \rangle &= \frac{1}{2} \iint m_i k k_c S(k_x, k_y) dk_x dk_y.\end{aligned}\quad (11)$$

The second of these is zero because of the symmetry of the spectrum about the wind direction. The expected value of the spectral modulation can therefore be written as

$$\hat{f} = m' \eta_u \quad \text{where} \quad m' = \langle f\eta_u \rangle / \sigma_u^2 = \frac{\iint m_i k k_u S(k_x, k_y) dk_x dk_y}{\iint k_u^2 S(k_x, k_y) dk_x dk_y}. \quad (12)$$

This expression is readily incorporated into the slope integral (1) by multiplying the SPM contributions by $1 + \hat{f}(\eta_u)$.

5. COMPARISON OF NUMERICAL AND ANALYTICAL RESULTS

Figure 1 shows a comparison of the analytical approximations discussed in Section 3 with results obtained by the numerical integration procedure discussed in Section 2. Both sets of calculations were made using a Gaussian slope probability density function (pdf). The large-scale slope variances and the SPM contributions were both calculated using the wave spectrum of Durden and Vesecky [7]. The expression $m' = -0.4/\sigma_u$ was used to produce a modulation transfer function similar to that used by Yueh [1].

The numerical slope integration was done in polar coordinates, with 90 angular and 50 slope subintervals, out to a maximum slope of 5σ , where σ is the rms slope (i.e., the square root of the total slope variance). The Stokes parameters were computed for 8 azimuth angles, and the results were used to calculate the Fourier harmonic coefficients by means of a least-squares fitting procedure. The time required to calculate each set of harmonic coefficients for a single wind speed was approximately 5 seconds on a 500 MHz Pentium processor, as compared to about 0.2 seconds for the analytical approximation.

As can be seen in Figure 1, the numerical and analytical results agree to within a few tenths of a degree K for low to intermediate wind speeds but begin to diverge at higher wind speeds, especially for U

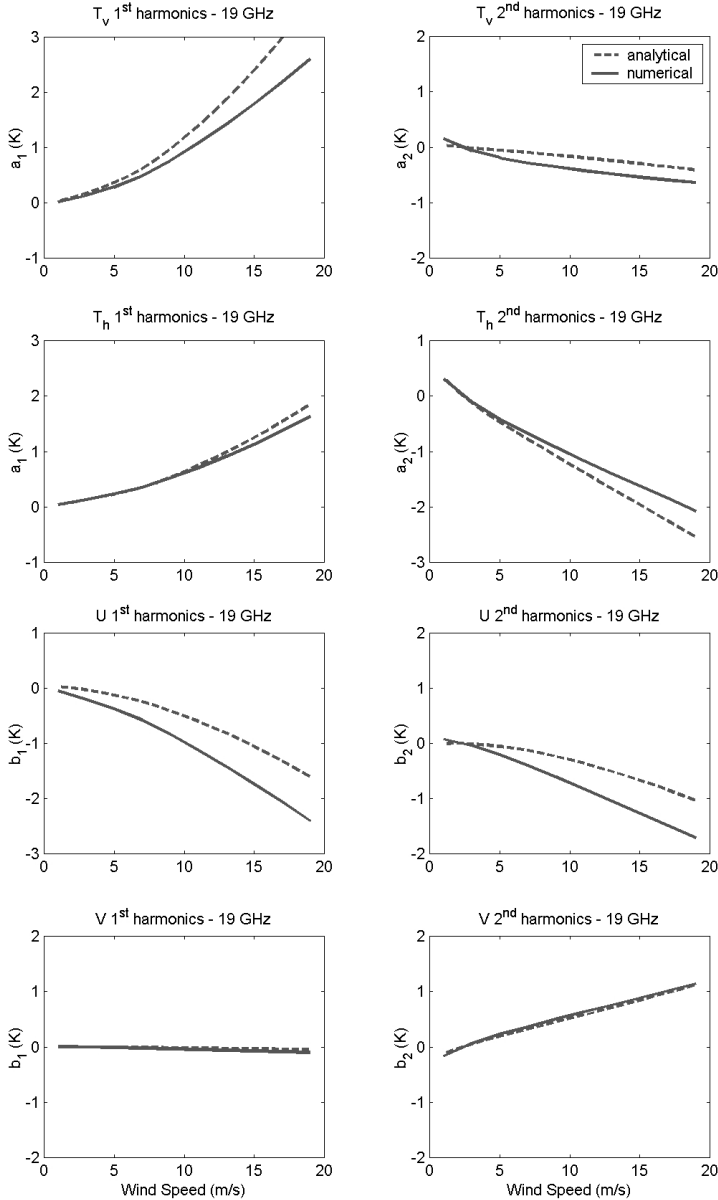


Figure 1. Comparison of analytical and numerical two-scale model results for a frequency of 19 GHz and an incidence angle of 55° , using a Gaussian slope pdf, the Durden-Vesecky spectrum, and a modulation transfer function similar to that of Yueh [1].

and T_v . This divergence presumably reflects the importance of higher-order derivatives of the SPM contributions, which were neglected in the analytical results shown here.

6. COMPARISONS WITH EXPERIMENTAL DATA

The measurements available for comparison with these calculations include those from the JPL Windrad instrument, as represented by the model functions reported by Yueh et al. [8], a large number of SSM/I observations analyzed by Wick et al. [9], and the results reported by Piepmeier and Gasiewski [10] using the airborne Polarimetric Scanning Radiometer. Comparisons between these results and the numerical predictions shown in Figure 1 showed differences in both the first and second harmonics, especially at high wind speeds. We therefore investigated various adjustments of the input parameters in order to improve the agreement.

The first harmonics were found to be governed primarily by the hydrodynamic mtf, while the second harmonics are dominated largely by the SPM contributions. To improve the agreement in the first harmonics, the imaginary part of the mtf was represented by the equation

$$m' = 0.1U_w - 2.5 \quad (13)$$

where U_w is the wind speed in m/s. We also used the asymmetric Gram-Charlier slope pdf, with the skewness coefficients reported by Cox and Munk [11], instead of the Gaussian distribution.

Improving the agreement between the predicted and observed second harmonics required a modification of the angular distribution of the short wave spectrum. Recent observations of the azimuthal dependence of the radar backscatter [12] also indicate that at high wind speeds the second Fourier harmonic of the backscatter is smaller than predicted by existing models such as Durden and Vesecky's. We therefore modified the Durden-Vesecky spectrum to produce a second harmonic equal to that observed by Donnelly et al. [12] at Ku-band and 50° incidence. Results using these parameters are compared with the experimental data in Figures 2 and 3 for frequencies of 19 and 37 GHz, and an incidence angle of 55° .

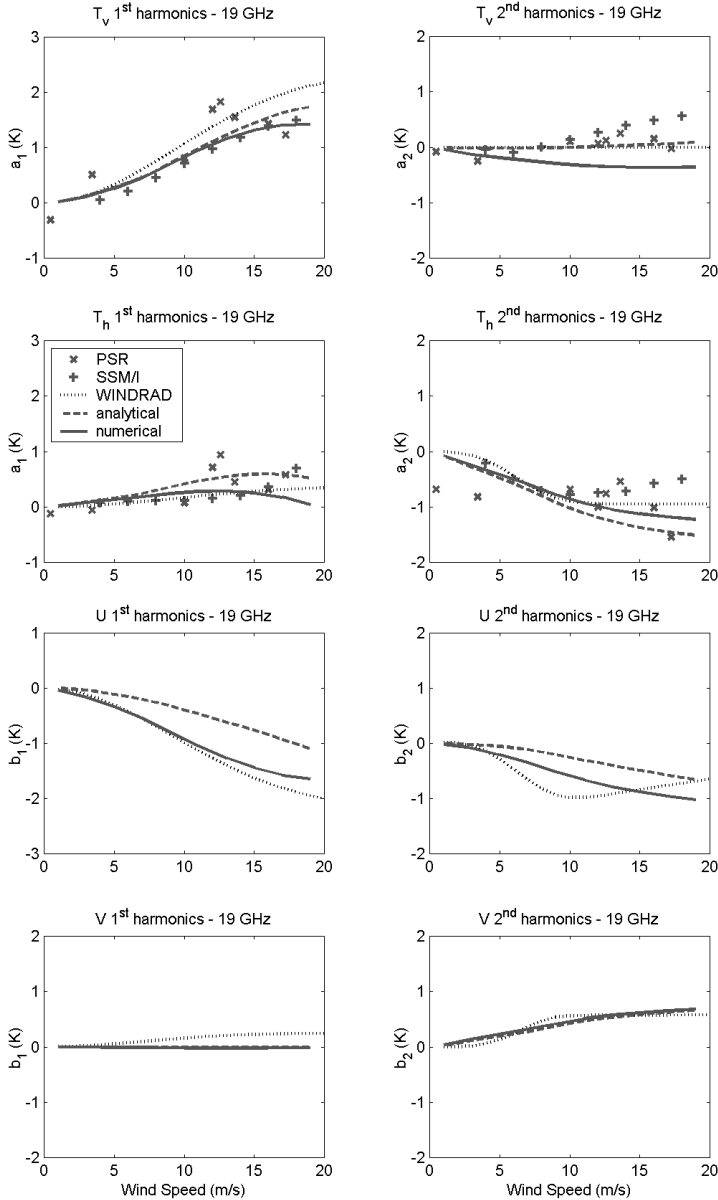


Figure 2. Comparison of experimental data with analytical and numerical two-scale model results for 19 GHz, using the modulation transfer function and spectrum described in the text, and a Gram-Charlier slope pdf with Cox and Munk's skewness coefficients.

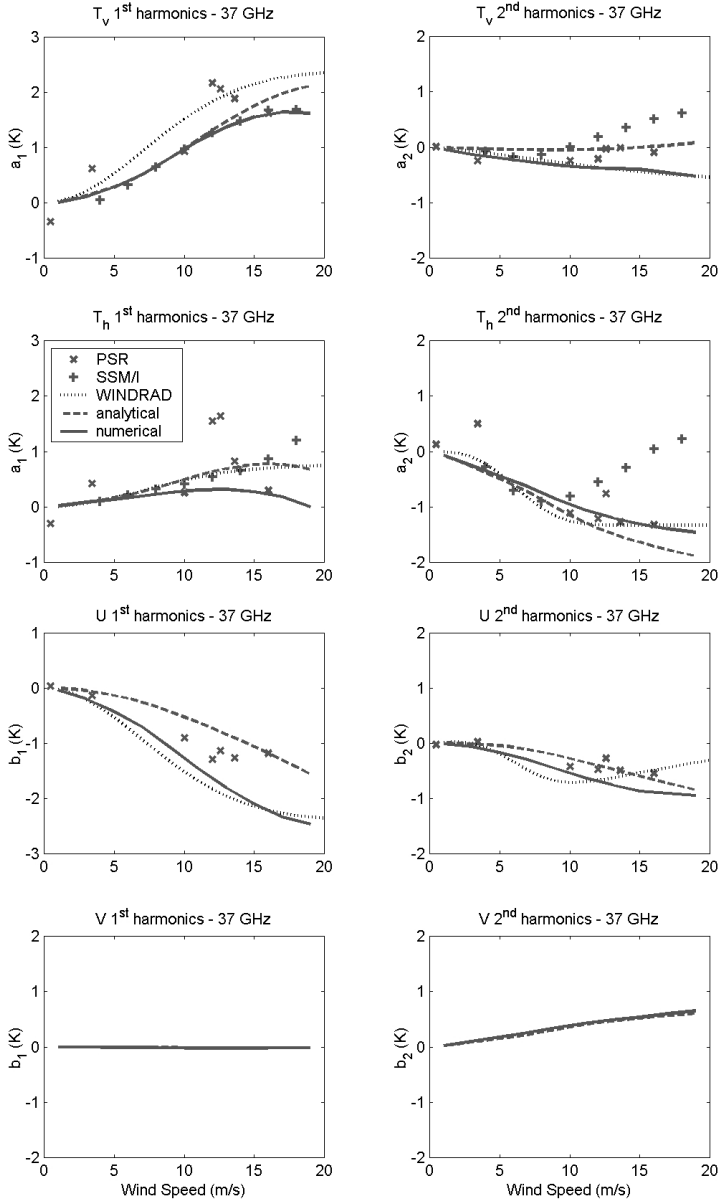


Figure 3. Comparison of experimental data with analytical and numerical two-scale model results for 37 GHz, using the modulation transfer function and spectrum described in the text, and a Gram-Charlier slope pdf with Cox and Munk’s skewness coefficients.

7. CONCLUSIONS

The differences between the predicted and observed values of the first and second harmonics of the Stokes parameters at 19 and 37 GHz are on the same order as the differences among the measurements, with the exception of the second harmonics inferred from SSM/I data by Wick et al. [10] at wind speeds above 10 m/s. The differences between the predicted second harmonics for T_v and the SSM/I values are considerable, especially at 37 GHz. On the other hand, the SSM/I values in this region are also much different from the aircraft measurements and from the values obtained by Wentz [13] using a different set of SSM/I observations.

It should be noted that our predictions do not include atmospheric effects, and these effects may explain some of the differences between the predictions and observations. Additional adjustment of various parameters such as the modulation transfer function and the slope probability density function may also improve the fit. Having optimized these parameters, we expect the physically based models described here to account for effects that are difficult to isolate using available measurements, such as the effects of surfactants and of atmospheric stability variations.

ACKNOWLEDGMENT

This work was supported by the Office of Naval Research under award number N00014-99-1-0174, Dr. Nahid Khazenie, technical monitor.

APPENDIX A. ANALYTICAL EXPRESSIONS FOR FOURIER HARMONICS

Using the approximations discussed in Section 3, the Stokes parameters can be represented by the Fourier series

$$\begin{aligned} T_v(\theta, \phi) &= A_{v0} + A_{v1} \cos \phi + A_{v2} \cos 2\phi, \\ T_h(\theta, \phi) &= A_{h0} + A_{h1} \cos \phi + A_{h2} \cos 2\phi, \\ U(\theta, \phi) &= B_{U1} \sin \phi + B_{U2} \sin 2\phi, \quad \text{and} \\ V(\theta, \phi) &= B_{V1} \sin \phi + B_{V2} \sin 2\phi \end{aligned}$$

where

$$A_{v0} = T_s[1 - \rho_v(\theta)] + \tau_v p_0 + a_{v0} - \left(a'_{v0} p_3 + \frac{1}{2} a'_{v2} p_4 \right) \tan \theta$$

$$\begin{aligned}
A_{v1} &= \frac{T_s}{4} \left[\frac{\rho_v - \rho_h}{\sin \theta \cos \theta} - \frac{1}{2}(\rho'_v(\theta) + 3\rho''_v(\theta) \tan \theta) \right] p_1 \\
&\quad + m' \left[\left(a'_{v0} + \frac{1}{2}a'_{v2} \right) - \left(a_{v0} + \frac{1}{2}a_{v2} \right) \tan \theta \right] \sigma_u^2 \\
A_{v2} &= a_{v2} + \frac{T_s}{2} \left[\frac{\rho_h - \rho_v}{\sin^2 \theta} + \frac{1}{2} \left(\rho'_v(\theta) \frac{\sin^2 \theta + 1}{\sin \theta \cos \theta} - \rho''_v(\theta) \right) \right] p_2 \\
&\quad - \frac{1}{2} (a'_{v0}p_4 + a'_{v2}p_3) \tan \theta \\
A_{h0} &= T_s[1 - \rho_h(\theta)] + \tau_h p_0 + a_{h0} - \left(a'_{h0}p_3 + \frac{1}{2}a'_{h2}p_4 \right) \tan \theta \\
A_{h1} &= \frac{T_s}{4} \left[\frac{\rho_h - \rho_v}{\sin \theta \cos \theta} - \frac{1}{2}(\rho'_h(\theta) + 2\rho''_h(\theta) \tan \theta) \right] p_1 \\
&\quad + m' \left[\left(a'_{h0} + \frac{1}{2}a'_{h2} \right) - \left(a_{h0} + \frac{1}{2}a_{h2} \right) \tan \theta \right] \sigma_u^2 \\
A_{h2} &= a_{h2} + \frac{T_s}{2} \left[\frac{\rho_v - \rho_h}{\sin^2 \theta} + \frac{1}{2} \left(\rho'_h(\theta) \frac{\sin^2 \theta + 1}{\sin \theta \cos \theta} - \rho''_h(\theta) \right) \right] p_2 \\
&\quad - \frac{1}{2} (a'_{h0}p_4 + a'_{h2}p_3) \tan \theta \\
B_{U1} &= \frac{T_s}{2} \left[\frac{\rho_h - \rho_v}{\sin \theta} + \frac{\rho'_v(\theta) - \rho'_h(\theta)}{\cos \theta} \right] p_1 + \frac{1}{2} m' [b'_{U2} - b_{U2} \tan \theta] \sigma_u^2 \\
B_{U2} &= b_{U2} T_s \left[\frac{\rho_v - \rho_h}{\sin^2 \theta \cos \theta} + \frac{\rho'_h(\theta) - \rho'_v(\theta)}{\sin \theta} \right] p_2 - \frac{1}{2} b'_{U2} p_3 \tan \theta \\
B_{V1} &= \frac{1}{2} m' [b'_{V2} - b_{V2} \tan \theta] \sigma_u^2 \quad \text{and} \quad B_{V2} = b_{V2} - \frac{1}{2} b'_{V2} p_3 \tan \theta.
\end{aligned}$$

In these expressions, a_{v0} etc. represent the SPM harmonic coefficients discussed in Section 2 and a'_{v0} etc. represent the derivatives of these harmonic coefficients with respect to the incidence angle. The p_n parameters are given by $p_0 = \sigma_u^2 + \sigma_c^2$, $p_1 = (c_{03}\sigma_u^2 + c_{21}\sigma_c^2)\sigma_u$, $p_2 = \sigma_u^2 - \sigma_c^2$, $p_3 = \sigma_u^2 + \sigma_c^2 + m'(c_{03}\sigma_u^2 + c_{21}\sigma_c^2)\sigma_u$ and $p_4 = \sigma_u^2 - \sigma_c^2 + m'(c_{03}\sigma_u^2 - c_{21}\sigma_c^2)\sigma_u$ where σ_u^2 and σ_c^2 are the upwind and crosswind slope variances and c_{03} and c_{21} are the Cox and Munk skewness coefficients. Finally, $\rho_v(\theta) = |R_v(\theta)|^2$ and $\rho_h(\theta) = |R_h(\theta)|^2$ are the Fresnel reflectivities, and $\tau_\alpha = \frac{1}{2} \left[\frac{\rho_\alpha(\theta) - \rho_\beta(\theta)}{\sin^2 \theta} + \frac{1}{2} (\rho'_\alpha(\theta) \frac{3 \sin^2 \theta - 1}{2 \sin \theta \cos \theta} - \rho''_\alpha(\theta)) \right] T_s$ where $\alpha = v$ or h and $\beta = h$ or v .

REFERENCES

1. Stogryn, A., "The apparent temperature of the sea at microwave frequencies," *IEEE Trans. Antennas Propagat.*, Vol. AP-15, No. 2, 278–286, March 1967.
2. Gasiewski, A. J. and D. B. Kunkee, "Polarized microwave emission from water waves," *Radio Sci.*, Vol. 29, No. 6, 1449–1466, Nov.–Dec. 1994.
3. Kunkee, D. B. and A. J. Gasiewski, "Simulation of passive microwave wind direction signatures over the ocean using an asymmetric-wave geometric optics model," *Radio Sci.*, Vol. 32, No. 1, 59–78, Jan.–Feb. 1997.
4. Camps, A. J. and S. C. Reising, "Wind direction azimuthal signature in the Stokes emission vector from the ocean surface at microwave frequencies," *Microwave and Optical Technology Letters*, Vol. 29, No. 6, 426–432, June 2001.
5. Yueh, S. H., "Modeling of wind direction signals in polarimetric sea surface brightness temperatures," *IEEE Trans. Geosci. Remote Sensing*, Vol. 35, No. 6, 1400–1418, Nov. 1997.
6. Yueh, S. H., R. Kwok, F. K. Li, S. V. Nghiem, and W. J. Wilson, "Polarimetric passive remote sensing of ocean wind vectors," *Radio Sci.*, Vol. 29, No. 4, 799–814, Jul.–Aug. 1994.
7. Durden, S. P. and J. F. Vesecky, "A physical radar cross-section model for a wind-driven sea with swell," *IEEE J. Oceanic Eng.*, Vol. OE-10, 445–451, Oct. 1985.
8. Yueh, S. H., W. J. Wilson, S. J. Dinardo, and F. K. Li, "Polarimetric microwave brightness signatures of ocean wind directions," *IEEE Trans. Geosci. Remote Sensing*, Vol. 37, No. 2, 949–959, Mar. 1999.
9. Wick, G. A., J. J. Bates, and C. C. Gottschall, "Observational evidence of a wind direction signal in SSM/I passive microwave data," *IEEE Trans. Geosci. Remote Sensing*, Vol. 38, No. 2, 823–837, Mar. 2000.
10. Piepmeier, J. R. and A. J. Gasiewski, "High-resolution passive polarimetric microwave mapping of ocean surface wind vector fields," *IEEE Trans. Geosci. Remote Sensing*, Vol. 39, No. 3, 606–622, Mar. 2001.
11. Cox, C. and W. Munk, "Measurement of the roughness of the sea surface from photographs of the sun's glitter," *J. Optical Soc. Am.*, Vol. 44, No. 11, 838–850, Nov. 1954.
12. Donnelly, W. J., J. R. Carswell, R. E. McIntosh, P. S. Chang, J. Wilkerson, F. Marks, and P. G. Black, "Revised ocean

- backscatter models at C and Ku band under high-wind conditions," *J. Geophys. Res.*, Vol. 104, No. C5, 11485–11497, May 1999.
13. Wentz, F. J., "Measurement of oceanic wind vector using satellite microwave radiometers," *IEEE Trans. Geosci. Remote Sensing*, Vol. 30, No. 5, 960–972, Sep. 1992.